Confinement Stabilizes a Bacterial Suspension into a Spiral Vortex

Hugo Wioland,[1] Francis G. Woodhouse,[1] Jörn Dunkel,[1] John O. Kessler,[2] and Raymond E. Goldstein[1]

[1] *Department of Applied Mathematics and Theoretical Physics, Centre for Mathematical Sciences, University of Cambridge, Wilberforce Road, Cambridge CB3 0WA, UK*
[2] *Department of Physics, University of Arizona, Tucson, AZ 85721, USA*

(Dated: April 9, 2013)

Confining surfaces play crucial roles in dynamics, transport and order in many physical systems, but their effects on active matter, a broad class of dynamically self-organizing systems, are poorly understood. We investigate here the influence of global confinement and surface curvature on collective motion by studying the flow and orientational order within small droplets of a dense bacterial suspension. The competition between radial confinement, self-propulsion, steric interactions and hydrodynamics robustly induces an intriguing steady single-vortex state, in which cells align in inwardly-spiralling patterns accompanied by a thin counterrotating boundary layer. A minimal continuum model is shown to be in good agreement with these observations.

PACS numbers: 87.18.Hf, 87.17.Jj, 47.63.Gd, 47.54.-r

Geometric boundaries and surface interactions are known to have profound effects on transport and order in condensed matter systems, with examples ranging from nanoscale edge currents in quantum Hall devices [1, 2] to macroscopic topological frustration in liquid crystals (LCs) tuned by manipulating molecular alignment at confining surfaces [3]. By contrast, in spite of considerable recent interest [4–8], the effects of external geometric constraints and confining interfaces on collective dynamics of *active* biological matter [9, 10], such as polar gels [11, 12] and bacterial [13–18] or algal suspensions [19], are not yet well understood, not least owing to a lack of well-controlled experimental systems.

At high concentrations, motile rod-like cells exhibit self-organization akin to nematic LC ordering [13, 14, 20], with the added facet of polar alignment driven by collective swimming [21, 22]. Unlike passive LCs, cellular suspensions are in a constant state of flux: at scales between 10 μm and 1 mm, coherent structures (swirls, jets, and plumes) continually emerge and persist for seconds at a time [14–17, 23]. While the dynamics of dense bacterial suspensions *in bulk* are fairly well understood [16, 18, 23–25], microorganisms often live in porous habitats like soil, where encounters with interfaces or three-phase contact lines are common [13, 14, 26]. Recent work has clarified how single cells interact with surfaces [27–30], but it remains unclear how global geometric constraints influence their collective motion.

Here we combine experiment and theory to investigate how confinement and boundary curvature affect stability and topology of collective dynamics in active suspensions. The physical system we study is an oil emulsion containing droplets of a highly concentrated aqueous suspension of *Bacillus subtilis* (Fig. 1a). For drops of diameter $d = 30$–$70\,\mu$m and height $h \sim 25\,\mu$m, we find that the suspension self-organizes into a single stable vortex (Fig. 1b) that persists as long as oxygen is available. This pattern is reminiscent of structures seen in colonies on the surface of agar [31], spontaneously circulating cytoplasmic extracts of algal cells [6], and the rotating interior of fibroblasts on micropatterned surfaces [32]. The vortex flow described here is purely azimuthal and accompanied by a thin counterrotating boundary layer, consisting of cells swimming opposite to the bulk. Surprisingly, we observe that the cells arrange in spirals with a maximum pitch angle of up to 35° relative to the azimuthal bulk flow direction (Fig. 1b). We suggest that this intriguing helical pattern results from the interplay of boundary curvature and steric and hydrodynamic interactions. Building on this hypothesis, we formulate a simple continuum model and find good agreement between its predictions and experimental results.

B. subtilis (wild-type strain 168) were grown in standard Terrific Broth (TB, Sigma) at 35° C on a shaker. An overnight culture was diluted 200× and grown for 5 h until the end of exponential growth when the proportion of motile cells is maximal [33]. Cells were then centrifuged at 1500g for 10 min. The pellet was gently mixed and transferred to 4 volumes of mineral oil, with 10 mg/mL diphytanoyl phosphatidylcholine (DiPhyPC, Avanti) added to prevent the emulsion from coalescing.

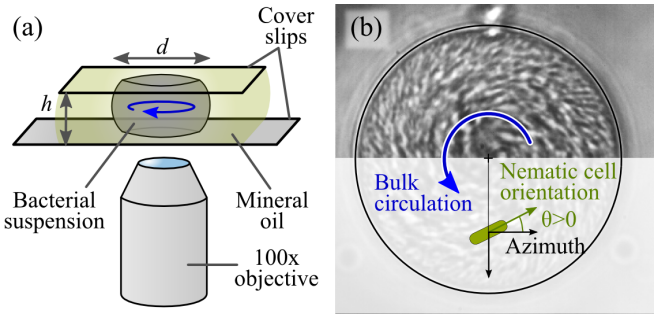

FIG. 1. (color online). Overview. (a) Experimental setup. (b) Bright field image of a 40 μm drop, and definition of cell orientation angle relative to main circulation direction.

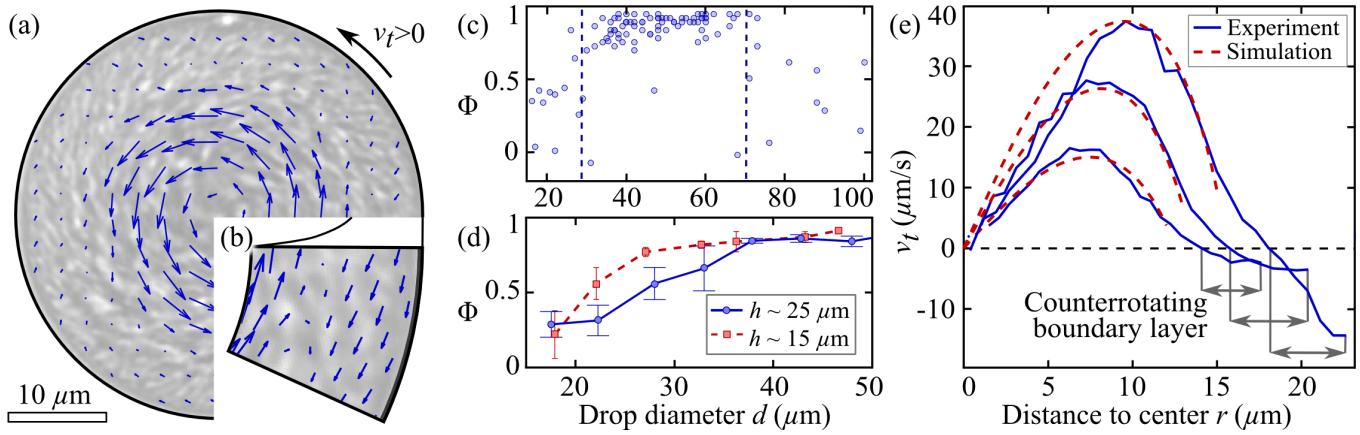

FIG. 2. (color online). Steady-state circulation in highly concentrated *B. subtilis* droplet. (a) PIV flow field for a droplet with a volume filling fraction $\varphi \sim 0.4$. For clarity, not all PIV vectors are shown. (b) Enlarged region reveals the counterrotating boundary layer. All PIV vectors are shown. (c-d) Vortex order parameter V for varying diameter d. (c) Drops of constant height $h \sim 25\,\mu$m. Dashed lines denote the highly ordered single-vortex regime. (d) Averaged vortex order parameter Φ ($5\,\mu$m bins) for $h \sim 15\,\mu$m (red dashed line) and $h \sim 25\,\mu$m (blue full line). Error bars indicate the standard deviation. (e) Azimuthal flow $v_t(r) = \langle \mathbf{v} \cdot \mathbf{t} \rangle_\theta$ profile for three different experiments (blue full lines), compared with continuum bulk flow model results (red dashed lines). Negative flow indicates the counterrotating boundary layer.

Small drops were created by slowly pipetting the suspension, $10\,\mu$L of which was placed between two coverslips such that it spread by surface tension to the coverslip edge. This procedure yields many flattened drops with $h \sim 25\,\mu$m and diameters ranging from 10–150 μm, and bacterial volume fraction $\varphi \sim 0.4$. Bacteria remain active for several minutes in the largest drops and up to 20 minutes for the smallest, reflecting the larger diffusive influx of oxygen in the smaller drops. Coverslips were rendered hydrophobic with silane, resulting in pancake-shaped drops that are wider at the midplane of the chamber than at the top and bottom (Fig. 1a). Movies were acquired at 125 fps with a high-speed camera (Fastcam, Photron) on an inverted microscope (Cell Observer, Zeiss), using a 100× oil-immersion objective and analyzed with custom Matlab algorithms. Flows were imaged in the center of the chamber to minimize optical distortions.

Confinement by the oil interface stabilizes rapidly rotating vortices (Fig. 2 and Supplemental Video 1). To quantify this effect, we determined the local bacterial velocity field $\mathbf{v}(\mathbf{x})$, using a customized version of the particle image velocimetry (PIV) toolbox mPIV [34] that averages pixel correlations over two seconds [35]. The PIV algorithm yields the local mean velocity of the bacteria, reflecting the locomotion due to swimming and advection by the fluid flow (Fig. 2a). The emergence of stable azimuthal flow is captured by the vortex order parameter

$$\Phi = \frac{\sum_i |\mathbf{v}_i \cdot \mathbf{t}_i| / \sum_j ||\mathbf{v}_j|| - 2/\pi}{1 - 2/\pi}, \qquad (1)$$

where $\mathbf{v}_i$ is the in-plane velocity and $\mathbf{t}_i$ the azimuthal unit vector (Fig. 1b) at PIV grid point $\mathbf{x}_i$. $\Phi = 1$ for steady azimuthal circulation, $\Phi = 0$ for disordered chaotic flows and $\Phi < 0$ for predominantly radial flows. Plotting Φ as a function of drop diameter reveals that a highly-ordered single-vortex state with $\Phi > 0.7$ forms if $d_- < d < d_+$ with $d_- \sim 30\,\mu$m and $d_+ \sim 70\,\mu$m (Fig. 2c). Clockwise and counterclockwise vortices occur with equal probability. The lower critical diameter d_- depends on the chamber height h (Fig. 2d). Lowering h restores the quasi-2D nature of the confinement and allows for formation of vortex states at smaller diameter d. The upper critical diameter d_+ is consistent with the size of the transient turbulent swirls observed in 3D bulk bacterial suspensions [16, 18, 24]. In drops slightly larger than d_+ flow is still azimuthal near the boundary regions but the vortex order decreases toward the center. Drops with $d \gtrsim 100\,\mu$m show fully developed bacterial turbulence as seen in quasi-infinite suspensions [14, 16, 18, 24].

The azimuthal flow speed in a vortex state is maximal at a distance $\sim d/4$ from the center (Fig. 2e). Across experiments, the maximum speed increases with d, reaching $\sim 40\mu$m/s for d_+, roughly four times the typical swimming speed of an isolated bacterium [17] and in agreement with measurements in open *B. subtilis* suspensions [16, 17]. While our setup does not supply oxygen, and the bacterial motility decreases [18] with time, recent studies of quasi-infinite suspensions [18, 24] have shown that the flow correlation length is independent of swimming speed at high cell density, so we may neglect oxygen depletion in the analysis of patterns. In the following, we focus on the properties of single-vortex states with $\Phi > 0.7$ and take the azimuthal unit vector $\mathbf{t}$ to point in the direction of bulk flow, so that we may treat clockwise and counterclockwise vortices equally (Fig. 1b).

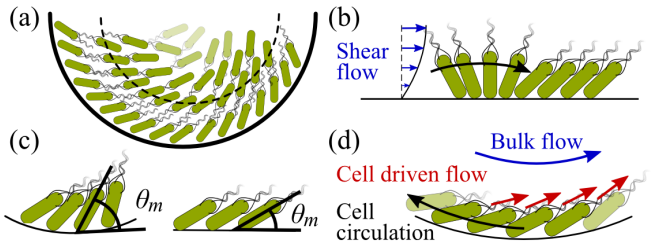

FIG. 3. (color online). Schematic cell organization in droplets. (a) Dashed line indicates continuum model boundary, where bulk flow begins. (b-d) Physical mechanisms driving boundary layer formation. (b) Shear flow reorients cells to face upstream. (c) Contact angle θ_m decreases with the drop diameter, restricted by steric interactions. (d) Ratchet-like steric repulsion and inward flow (red arrows) created by boundary cells force the next layer to move in the opposite azimuthal direction, thereby setting the bulk flow direction.

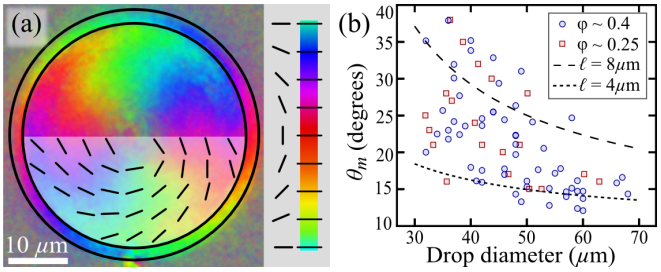

FIG. 4. (color online). Bacterial orientation. (a) Local orientation, averaged over 2 s. External ring lies at the water/oil interface and shows local azimuthal direction, and cellular orientation appears in the central disc. Discontinuity in color between ring and disc indicates the angle between cells and the azimuthal direction. (b) Boundary angle (Fig. 3c) as a function of drop diameter, Symbols denote different bacterial concentrations; dashed black lines indicate geometric estimates of minimum packing angle Θ for different cell lengths.

Detailed flow field analysis reveals that highly ordered vortex states are always accompanied by a thin layer of cells swimming along the oil interface in the opposite direction to the bulk flow (Fig. 2b). This surprising fact is reflected in the azimuthally-averaged circulation velocity profile $v_t(r) = \langle \mathbf{v}(\mathbf{x}) \cdot \mathbf{t} \rangle_\theta$, where $\mathbf{x} = (r\cos\theta, r\sin\theta)$, which changes sign towards the edge of the droplet (Fig. 2e). The basic form of $v_t(r)$ is preserved among well-ordered droplets ($\Phi > 0.7$) with different diameters (Fig. 2e). To exclude the possibility that the backflow arises from specific interactions between bacteria, DiPhyPC and oil, we performed control experiments with dense suspensions in shallow cylindrical polydimethylsiloxane chambers, and found qualitatively similar behavior. This result suggests that the formation of a thin counterflow boundary layer is a generic phenomenon in bacterial suspensions confined by a higher-viscosity medium. By determining the zeros of v_t for all ordered droplets, we find that the boundary layer thickness b is independent of d (Fig. 2e). The average value $\bar{b} \approx 4\,\mu$m is slightly smaller than the length $\ell \approx 5\,\mu$m of *B. subtilis* [23], suggesting that the counterflow region is comprised of a single layer of cells. We tested this hypothesis by imaging droplets in a plane near the bottom cover slip in order to resolve vertical cell layers more easily, and confirmed that cells swimming in the direction opposite to the bulk flow are in direct contact with the oil interface (Fig. 3a and Supplemental Video 2).

The presence of this previously unreported counterflow layer can be understood by considering the main forces that cause reorientation of cells near the boundary. Since the oil viscosity is ten times that of water, the interface acts as a nearly-no-slip boundary for the suspension. Thus, circular bulk motion creates a shear flow that exerts torque on the cells in the boundary layer (Fig. 3b). As recently shown for dilute suspensions [36], bacteria prefer to swim upstream when exposed to such flow gradients, thereby favoring the formation of a counterrotating layer. If the concentration of cells is sufficiently high, nematic ordering due to steric interactions further stabilizes this layer [10, 21, 22]. Once the layer has formed, cells trapped in it form a steric ratchet-like structure and, because they are pusher-type swimmers [30], they generate a backflow in the direction opposite to their orientation (Fig. 3d). Both effects force cells in the second layer to move in the other direction: the boundary monolayer stabilizes the bulk flow and *vice versa*. The absence of such counter-circulation in the free-boundary geometry studied by Czirok *et al.* [31] provides further evidence that the backflow is a consequence of rigid boundary effects.

A dense suspension of rod-like bacteria locally aligns through active nematic interactions [10, 21, 22]. We observe cell orientation that is not parallel to the flow direction: in the bulk circulation the cells point inwards, and in the boundary layer they point outwards (Fig. 3a). We extract the local mean orientation from the bacterial speckle by computing the orientation tensor [37] (Fig. 4a). As for the flow, we examine the azimuthally-averaged orientation angle $\theta(r)$ relative to the circulation direction $\mathbf{t}$. Near the center of a drop, cells are aligned roughly parallel to the bulk circulation ($\theta \approx 0$), and the angle increases with r to a maximum value θ_m close to the boundary. Viewing θ_m as a function of d, we find an inverse correlation: the smaller the drop (and thus the higher the boundary curvature), the larger the deviation from the azimuthal direction, ranging from $\theta_m \sim 10^\circ$ for $d = 70\,\mu$m to $\theta_m \sim 35^\circ$ for $d = 30\,\mu$m (Fig. 4b). To test whether θ_m depends on the curvature or on the suspension size, we performed measurements with suspensions diluted to $\sim 2/3$ of the starting concentration. In such a drop, cells concentrate at the boundary, leaving the center almost empty (Supplemental Video 3). Yet, the measured angles are comparable to those of fully concentrated suspensions (Fig. 4b), indicating that this is

indeed an effect of boundary curvature.

To explain this phenomenon qualitatively, we consider purely steric bacterial packing in the boundary layer. This viewpoint is supported by the simulations of Wensink and Löwen [5] which show that a group of self-propelled particles does not align parallel to a boundary but instead lies at an angle limited by steric repulsion. Given a bacterial concentration, we model cells as thin rectangles equally spaced around a circle of diameter d and then calculate the minimum packing angle Θ with the azimuthal direction at which the cells could lie in one plane. A dilute suspension thus has edge-parallel packing ($\Theta = 0°$), while at some limiting concentration they become boundary-perpendicular ($\Theta = 90°$). In the intermediate regime, Θ decreases as drop diameter d increases (i.e., as boundary curvature falls; Fig. 3c). Figure 4b illustrates packing curves for two cell lengths, $\ell = 4\,\mu$m and $\ell = 8\,\mu$m, at a volume fraction of 0.5. The measured values of θ_m then lie between these two curves, indicating that the scatter can be explained by variations in the cell length ℓ (which are also observed across experiments).

While single-field phenomenological models can describe dense bacterial flow quantitatively [23, 24], they do not incorporate the additional observable of cellular orientation. Thus, as is typical in active suspension theory [38] we describe the system by two functions: the bacterial polar order parameter $\mathbf{P}$, where $|\mathbf{P}| = 0$ for total disorder and $|\mathbf{P}| = 1$ for total order in direction $\mathbf{P}$, and the suspending fluid flow $\mathbf{u}$. The fluid obeys the forced Stokes equations with friction,

$$-\mu\nabla^2\mathbf{u} + \nu\mathbf{u} + \nabla\Pi = -c_0\sigma\nabla\cdot(\mathbf{PP}),$$

and incompressibility $\nabla\cdot\mathbf{u} = 0$. The viscosity μ and coefficient of friction ν (from the effects of high bacterial density) control the fluid response to dipolar 'pusher' forcing (strength σ) in a suspension of concentration c_0. Defining the incompressible *swimming field* functional $\mathbf{s}[\mathbf{P}]$, $\nabla\cdot\mathbf{s} = 0$, the polar order $\mathbf{P}$ evolves as

$$\partial_t\mathbf{P} + (\mathbf{u}+\mathbf{s})\cdot\nabla\mathbf{P} = D_s\nabla^2\mathbf{P} - D_r\mathbf{P} + \alpha(1-|\mathbf{P}|^2)\mathbf{P} + \epsilon(\mathbb{I}-\mathbf{PP})\cdot(\gamma\mathbf{E}+\mathbf{W})\cdot\mathbf{P}.$$

On the l.h.s, cells are advected by a flow field $\mathbf{u}+\mathbf{s}$, where in general, $\mathbf{s}$ is proportional to the incompressible part of $\mathbf{P}$. This ensures that concentration fluctuations always dissipate, as appropriate for a highly dense suspension. On the r.h.s., the terms are, in order: spatial and rotational diffusion with respective constants D_s and D_r; spontaneous polar ordering of strength α; and reorientation induced by solvent strain $\mathbf{E} = (\nabla\mathbf{u} + \nabla\mathbf{u}^{\mathsf{T}})/2$ and vorticity $\mathbf{W} = (\nabla\mathbf{u} - \nabla\mathbf{u}^{\mathsf{T}})/2$, with cell shape parameter $\gamma \in [-1, 1]$ and effectiveness $\epsilon \leq 1$ (inhibited by steric effects). The presence of a bacterial boundary layer in a circular bulk flow is mimicked by imposed boundary conditions at $r = d_0/2$ of fixed orientation $\mathbf{P} = \mathbf{t}\cos\theta_b - \mathbf{r}\sin\theta_b$, where $\mathbf{r}$ is the outward radial unit vector. A no-slip boundary condition is imposed on the fluid flow. (A systematic treatment of this model with appropriate nondimensionalizations will be presented elsewhere; here we retain the fully dimensional parameters for simpler connection with experiments.)

To model the steady vortex regime we reduce to axisymmetry, where $\mathbf{u} = u\mathbf{t}$ and $\mathbf{s} = s\mathbf{t}$ by incompressibility. We then set $s = V\mathbf{P}\cdot\mathbf{t}$ for azimuthal swimming at speed V. To model the results in Fig. 2d, we fix appropriate parameter values [30] $c_0 = 0.1\,\mu\text{m}^{-3}$, $\mu = 10^{-3}\,\text{Pa}\,\text{s}$, $\nu = 10^{-4}\,\text{Pa}\,\text{s}\,\mu\text{m}^{-2}$, $D_s = 10^3\,\mu\text{m}^2\,\text{s}^{-1}$, $D_r = 0.057\,\text{s}^{-1}$, $\alpha = 25\,\text{s}^{-1}$, $\epsilon = 0.5$, $\gamma = 0.9$, and $\theta_b = 20°$. We then choose three bulk domain diameters $d_0 = 24, 26, 30\,\mu$m, and for each we pick $V = 4, 7, 10\,\mu\text{m}\,s^{-1}$ and $\sigma = 0.3, 0.525, 0.75\,\text{pN}\,\mu$m respectively, reflecting varying oxygen availability. These yield the steady-state curves of the lab frame bacterial flow $|\mathbf{u}+\mathbf{s}|$ shown in Fig. 2c, exhibiting good agreement in the bulk flow regime. Additionally, the orientation angle $\theta(r)$ decreases towards zero from its initial value $\theta(d_0/2) = \theta_b$ as r decreases, as observed experimentally (Fig. 4a).

The overall bacterial arrangement we have observed is reminiscent of rotating spirals predicted for totally ordered active gels [12], although that model describes the actin-myosin cytoskeleton and lacks interactions particular to microswimmer suspensions [39]. A more appropriate representation could be derived from polar active liquid crystals: the bacterial boundary layer could be regarded as a smectic structure [40] while the bulk behaves as a chiral nematic phase [3]. Yet, it is only by considering the microscopic hydrodynamics near the oil interface that the presence of the backflow layer can be inferred. This lends a note of caution to continuum modeling of microswimmer suspensions, suggesting that conditions at boundaries, and microscopic effects in general, warrant careful and deliberate consideration. Our combined experimental and theoretical results demonstrate that suitably designed boundaries provide a means for stabilizing and controlling order in active microbial systems.

We thank A. Honerkamp-Smith, V. Kantsler, P. Khuc Trong, K. Leptos and E. Lushi for discussions. This work was supported by the EPSRC and ERC Advanced Investigator Grant 247333.

[1] K. von Klitzing, Physica B **184**, 1 (1993).
[2] A. H. MacDonald and P. Středa, Phys. Rev. B **29**, 1616 (1984).
[3] D. Seč, T. Porenta, M. Ravnik, and S. Žumer, Soft Matter **8**, 11982 (2012).
[4] D. Grossman, I.S. Aranson, and E.B. Jacob, New J. Phys. **10**, 023036 (2008).
[5] H.H. Wensink and H. Löwen, Phys. Rev. E. **78**, 031409 (2008).
[6] F.G. Woodhouse and R.E. Goldstein, Phys. Rev. Lett.

109, 168105 (2012).
[7] M. Ravnik and J.M. Yeomans, Phys. Rev. Lett. **110**, 026001 (2013).
[8] T. Brotto, J.-B. Caussin, E. Lauga, and D. Bartolo, Phys. Rev. Lett. **110**, 038101 (2013).
[9] D.L. Koch and G. Subramanian, Annu. Rev. Fluid Mech. **43**, 637 (2011).
[10] T. Vicsek, A. Cziròk, E. Ben-Jacob, I. Cohen, and O. Shochet, Phys. Rev. Lett. **75**, 1226 (1995).
[11] S. Fürthauer, M. Neef, S. W. Grill, K. Kruse, and F. Jülicher, New J. Phys. **14**, 023001 (2012).
[12] K. Kruse, J.F. Joanny, F. Jülicher, J. Prost, and K. Sekimoto, Phys. Rev. Lett. **92**, 078101 (2004).
[13] J.O. Kessler and M. F. Wojciechowski, in *Bacteria as Multicellular Organisms*, ed. by J. A. Shapiro and M. Dworkin (Oxford University Press, New York, 1997), p. 417.
[14] C. Dombrowski, L. Cisneros, S. Chatkaew, R.E. Goldstein, and J.O. Kessler, Phys. Rev. Lett. **93**, 098103 (2004).
[15] I. Tuval, L. Cisneros, C. Dombrowski, C.W. Wolgemuth, J.O. Kessler, and R.E. Goldstein, Proc. Natl. Acad. Sci. U.S.A. **102**, 2277 (2005).
[16] L.H. Cisneros, R. Cortez, C. Dombrowski, R.E. Goldstein, and J.O. Kessler, Exp. Fluids **43**, 737 (2007).
[17] A. Sokolov, I.S. Aranson, J.O. Kessler, and R.E. Goldstein, Phys. Rev. Lett. **98**, 158102 (2007).
[18] A. Sokolov and I.S. Aranson, Phys. Rev. Lett. **109**, 248109 (2012).
[19] S. Rafai, L. Jibuti, and P. Peyla, Phys. Rev. Lett. **104**, 098102 (2010).
[20] D.Volfson, S. Cookson, J. Hasty, and L.S. Tsimring, Proc. Natl. Acad. Sci. U.S.A. **105**, 15346 (2008).
[21] F. Ginelli, F. Peruani, M. Bär, and H. Chaté, Phys. Rev. Lett. **104**, 184502 (2010).
[22] H.H. Wensink, and H. Löwen, J. Phys.: Condens. Matter **24**, 46413 0(2012).
[23] H.H. Wensink, J. Dunkel, S. Heidenreich, K. Drescher, R.E. Goldstein, H. Löwen, and J.M. Yeomans, Proc. Natl. Acad. Sci. U.S.A. **109**, 14308 (2012).
[24] J. Dunkel, S. Heidenreich, K. Drescher, H.H. Wensink, M. Bär, and R.E. Goldstein, arXiv:1302.5277 (2013).
[25] E. Lushi, and C.S. Peskin, Comput. Struct., in press (2013).
[26] W.M. Durham, O. Tranzer, A. Leombruni, R. Stocker, Phys. Fluids **24**, 091107 (2012).
[27] W.R. DiLuzio, L. Turner, M. Mayer, P. Garstecki, D.B. Weibel, H.C. Berg, and G.M. Whitesides, Nature **435**, 1271 (2005).
[28] G. Li and L.-K. Tam and J. X. Tang, Proc. Natl. Acad. Sci. U.S.A. **105**, 18355 (2008).
[29] V. Kantsler, J. Dunkel, M. Polin, and R.E. Goldstein, Proc. Natl. Acad. Sci. U.S.A. **110**, 1187 (2013).
[30] K. Drescher, J. Dunkel, L.H. Cisneros, S. Ganguly, and R.E. Goldstein, Proc. Natl. Acad. Sci. U.S.A. **108**, 10940 (2011).
[31] A. Czirók, E. Ben-Jacob, I. Cohen, and T. Vicsek, Phys. Rev. E **54**, 1791 (1996).
[32] A. Kumar, A. Maitra, M. Sumit, G.V. Shivashankar, and S. Ramaswamy, arxiv:1302.6052.
[33] D.B. Kearns and R. Losick, Gene Dev. **19**, 3083 (2005).
[34] N. Mori and K.-A. Chang (2006); For details, see www.oceanwave.jp/softwares/mpiv_doc.
[35] C.D. Meinhart, S.T. Wereley, and J.G. Santiago, J. Fluid. Eng. **122**, 285 (2000).
[36] J. Hill, O. Kalkanci, J.L. McMurry, and H. Koser, Phys. Rev. Lett. **98**, 068101 (2007).
[37] R. Rezakhaniha *et al.*, Biomech. Model. Mechan. **11**, 461 (2011).
[38] D. Saintillan and M.J. Shelley, Phys. Rev. Lett. **100**, 178103 (2008).
[39] J.-F. Joanny and J. Prost, HFSP J. **3**, 94 (2009).
[40] L. Giomi, M.C. Marchetti, and T.B. Liverpool, Phys. Rev. Lett. **101**, 198101 (2008).